CHEMISTRY OF MATERIALS

pubs.acs.org/cm

Article

Computational Investigation of Halogen-Substituted Na Argyrodites as Solid-State Superionic Conductors

Bin Ouyang, Yan Wang, Yingzhi Sun, and Gerbrand Ceder*

Cite This: *Chem. Mater.* 2020, 32, 1896–1903

Read Online

ACCESS | Metrics & More | Article Recommendations | Supporting Information

ABSTRACT: The discovery of promising inorganic superionic conductors for use as solid-state electrolytes can enable the design of safe and high-energy-density solid-state batteries. Li argyrodites with the composition Li–P–S–X (X = Cl, Br, or I) have been found to have an ionic conductivity of up to 14.8 mS/cm, indicating the ability of the argyrodite framework to conduct alkali-metal ions. However, the sodium version of argyrodites remains unexplored. In this work, using first-principles density functional theory calculations, we examine the phase stability, electrochemical stability, and ionic conductivity of 48 potential Na argyrodites with different pnictogen, chalcogen, and halogen chemistries and site occupancies. We find that for sulfide-based Na argyrodites, the compounds with halogens occupying both the 4a and 4c sites typically display better ionic conductivity. However, the larger size of the Se^{2-} anion makes selenide-based Na argyrodites less-dependent on the exact halogen-site occupancy. Most of the Na argyrodites have positive zero-K formation energy but are within the typical energy where compounds, including the Li argyrodite, can be synthesized. We find that compounds within the Na–P–Se–X (X = Cl, Br, or I) chemical space may form a good compromise between ionic conductivity, phase stability, and synthesizability.

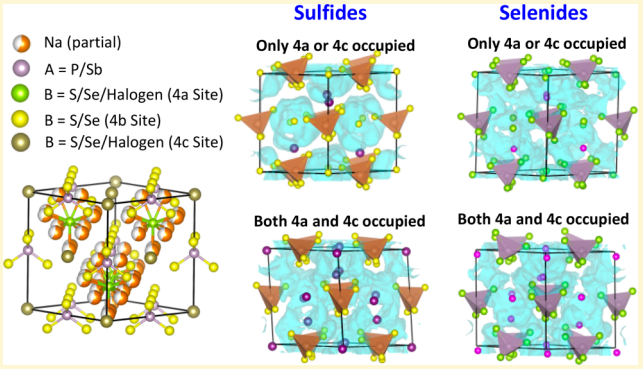

1. INTRODUCTION

Solid-state batteries show great potential for improved safety as they replace the flammable liquid electrolyte in conventional Li- and Na-ion batteries by a nonflammable solid electrolyte. The recent rapid development of solid-state electrolytes has been driven by the successful search for materials that are superionic Li or Na conductors at room temperature.[1−16] For Li superionic conductors, several frameworks have been identified as being well-suited for Li transport, including Li garnets,[5,6,17] antiperovskites,[14−16] $Li_{10}GeP_2S_{12}$-type materials,[3,11] Li phosphorus sulfides ($Li_7P_3S_{11}$, β-Li_3PS_4, and Li_2S–P_2S_5 ceramic glasses),[10,12,18] and Li argyrodites.[19−22]

However, far fewer promising Na superionic conductors have been identified. As certain anion frameworks[2,13] have been demonstrated to show great capability for conducting Li, it is reasonable to examine the suitability of these anion frameworks for conducting Na.[8] Li argyrodites with the chemical formula Li_6PS_5Cl or $Li_5PS_4Cl_2$, originating from the prototype Ag_8GeS_6, have been shown both theoretically and experimentally to be capable of delivering ionic conductivities greater than 14.8 mS/cm.[19,21−26] However, to date, there have been no studies on the possibility of using this framework for conducting Na.

In this work, first-principles computational techniques are applied to evaluate the potential of Na argyrodites for fast Na-ion transport. We study different pnictogen (P or Sb), chalcogen (S or Se), and halogen (Cl, Br, or I) combinations and investigate the effect of varying site occupancies on the halogen site. Phase stability, electrochemical stability, and ionic conductivity of 48 types of Na argyrodites are investigated allowing us to identify promising Na argyrodites with reasonable stability and ionic conductivity. The occupancy distribution of the halogen over one of the chalcogen sites is observed to have a significant effect on the Na conductivity in sulfide-based Na argyrodites. When a halogen occupies both loosely bonded chalcogen sites, the ionic conductivity is greatly improved. However, this site-occupancy dependency is not observed for selenide-based argyrodites. Combining both ionic conductivity and phase stability, our findings indicate that it would be most promising to design superionic Na argyrodites in the Na–P–Se–X (X = Cl, Br, or I) compositional space.

2. METHODOLOGY

2.1. Density Functional Theory Structural Optimization and Total Energy Calculations. The possible structure

Received: November 4, 2019
Revised: February 5, 2020
Published: February 6, 2020

https://dx.doi.org/10.1021/acs.chemmater.9b04541
Chem. Mater. 2020, 32, 1896–1903

of Na argyrodites without halogen substitution, Na_7AB_6, is derived from the structure of Li_7PS_6,[27] with Li being substituted by Na, and is shown in Figure 1. There are 12

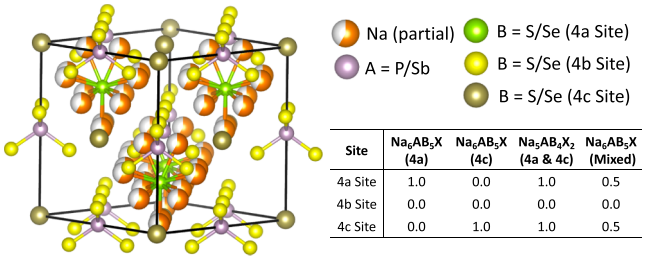

Site	Na_6AB_5X (4a)	Na_6AB_5X (4c)	$Na_5AB_4X_2$ (4a & 4c)	Na_6AB_5X (Mixed)
4a Site	1.0	0.0	1.0	0.5
4b Site	0.0	0.0	0.0	0.0
4c Site	0.0	1.0	1.0	0.5

Figure 1. Structure of Na argyrodites. The A atom can be either P or Sb, and the B atom can be either S or Se. When a halogen is introduced, it will replace S/Se at the 4a/4c sites. Depending on the halogen (X = Cl, Br, and I)-occupying site, four types of Na argyrodites are formed, and the halogen occupancy in all sites is indicated in the embedded table.

possible Na sites per formula unit. Because of the possible partial occupancy of the Na sites, we evaluated the electrostatic energy of all possible Na arrangements in a supercell with 48 Na sites and used the structure with the lowest electrostatic energy in further density functional theory (DFT) calculations. Total energies and molecular dynamics simulations were performed with the Vienna ab initio simulation package (VASP) with a plane-wave basis set.[28] Projector augmented wave potentials with a kinetic energy cutoff of 520 eV and the exchange−correlation form in the Perdew−Burke−Ernzerhof-generalized gradient approximation[29] were employed in all the structural optimizations and total-energy calculations. For all the calculations, a reciprocal space discretization of 25 k-points per $Å^{-1}$ was applied, and the convergence criteria were set as 10^{-6} eV for electronic iterations and 0.02 eV/Å for ionic iterations.

2.2. Phase Stability and Electrochemical Stability Analysis. The thermodynamic stability of the possible Na argyrodites was evaluated by constructing the convex hull of the DFT total energy for all phases in the relevant chemical space available in an internal database which contains phases from the Inorganic Crystal Structure Database (ICSD) and some compounds generated using data-mined substitution rules.[30] The convex hull ensures that each ground state has an energy lower than any linear combination of phases that leads to the same composition as the ground state. Phase stability for phases not on the hull is quantified by their energy above the hull (E_{hull}), which indicates the compound's driving force for decomposition into other ground states. E_{hull} serves as a reasonable indicator of synthetic accessibility, as experimentally accessible materials must generally have a low energy above the hull.[31]

Electrochemical phase stability is evaluated from grand canonical phase diagrams following previous work.[7,32−35] For any sodium chemical potential μ_{Na}, we consider the grand potential Φ

$$\Phi[c, \mu_{Na}] = E[c] - n\mathrm{Na}[c]\mu_{Na} \quad (1)$$

where c is the composition of the material, $E[c]$ is the enthalpy per formula unit, and $n\mathrm{Na}[c]$ is the number of Na atoms per formula unit. Given that argyrodites are metastable phases that can be stabilized by both configurational and vibrational entropy at high temperature, the enthalpy of Na argyrodites was set to the convex hull energy at their composition when evaluating the electrochemical stability window. The range of μ_{Na}, $[\mu_{Red}, \mu_{Ox}]$, over which the material is stable in the grand potential phase diagram can be converted into the electrochemical stability window $[V_{Red}, V_{Ox}]$ by referencing the chemical potential to the energy of the Na metal.[36−38]

2.3. Na-Ion Diffusivity and Conductivity Calculations. Ab initio molecular dynamics (AIMD), initialized from the lowest-energy atomic configurations, was used to investigate the ionic conductivity. All the AIMD calculations are performed in an *NVT* ensemble with a time step of 1 fs and using a Nosé−Hoover thermostat[39] for a period of 100 ps. For compounds with very low diffusivity, such as the Na−Sb−S−X systems, an AIMD simulation of 200 ps is used to ensure good statistics. A minimal Γ-point-only k-point grid was used with spin-polarized calculations. The AIMD simulations were run at 600, 800, 900, 1000, 1100, and 1200 K. All the data were fitted assuming Arrhenius behavior to obtain the activation energy, diffusion prefactor, and room-temperature diffusivity.

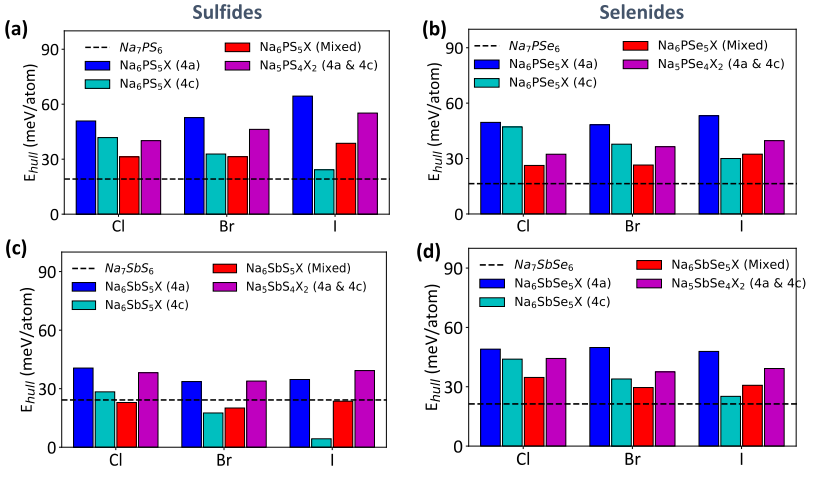

Figure 2. Phase stability (energy above the hull, E_{hull}) of Na argyrodites in the (a) Na−P−S−X, (b) Na−P−Se−X, (c) Na−Sb−S−X, and (d) Na−Sb−Se−X compositional spaces.

https://dx.doi.org/10.1021/acs.chemmater.9b04541
Chem. Mater. 2020, 32, 1896−1903

Table 1. Predicted Competing Phases (Decomposition Products) of Different Na Argyrodites from Phase Diagram Analysis, X Refers to Cl, Br, or I

formula	competing phases	formula	competing phases
Na_6PS_5X	$NaX + Na_2S + Na_3PS_4$	Na_6SbS_5X	$NaX + Na_2S + Na_3SbS_4$
$Na_5PS_4X_2$	$NaX + Na_3PS_4$	$Na_5SbS_4X_2$	$NaX + Na_3SbS_4$
Na_6PSe_5X	$NaX + Na_2Se + Na_3PSe_4$	Na_6SbSe_5X	$NaX + Na_2Se_2 + Na_3SbSe_3$
$Na_5PSe_4X_2$	$NaX + Na_3PSe_4$	$Na_5SbSe_4X_2$	$NaX + Na_2Se_2 + NaSbSe_2$

3. RESULTS

3.1. Phase Stability. As illustrated in Figure 1, in the argyrodite formula Na_7AB_6, A refers to a pnictogen atom (either P or Sb) and B is typically a chalcogen atom such as S and Se. There are three types of anion sites in the argyrodite structure, which are usually denoted as 4a, 4b, and 4c. The chalcogen at the 4b site creates a covalent bond with the pnictogen to form AB_4 polyanions. However, anions at the 4a and 4c sites are loosely bonded and only have Na in their first coordination shell. When a halogen atom is introduced, it preferentially occupies 4a or 4c sites.[20,21,23] Thus, we considered four types of argyrodites depending on the occupancy of these sites, as indicated in the table embedded in Figure 1. When the 4a or 4c sites are fully occupied by halogens, the configurations are denoted as "4a" and "4c", respectively. When half of the 4a sites and half of the 4c sites are occupied by halogens, the configuration is denoted as "mixed". All three configurations have the same composition with the formula Na_6AB_5X. With increasing halogen substitution, the 4a and 4c sites will eventually be fully substituted by halogens, yielding the chemical formula $Na_5AB_5X_2$. We also consider this case because a recent study showed that this level of halogen substitution can be achieved in Li argyrodites.[23,40]

The calculated E_{hull} values for all the studied Na argyrodites are shown in Figure 2. The E_{hull} values for the different site occupancies are colored differently. The E_{hull} value of the corresponding argyrodites without substitution (Na_7AB_6) is indicated by the horizontal dashed lines. Several pieces of information can be inferred from the results shown in Figure 2. First, the sulfide- and selenide-based Na argyrodites generally have lower E_{hull} values than Li_7PS_6 (calculated to be ~37 meV/atom). Additionally, with halide substitution, the E_{hull} of many Na argyrodites remains less than that of Li_7PS_6. For some compositions, such as Na_6PS_5I with I in the 4a sites, E_{hull} is only 4.34 meV/atom. As demonstrated in Table 1, the competing phases on the hull are sodium halides (NaX), sodium chalcogenides (Na_2S/Na_2Se), and Na_3AB_4 except for Na−Sb−Se−X systems, for which Na_2Se_2, Na_3SbSe_3, and $NaSbSe_2$ are the competing phases. Given that Li argyrodites typically have E_{hull} values of over 20 meV/atom with Li halides, Li sulfides, and Li_3PS_4 as competing phases,[40] this finding indicates that many of the Na argyrodites considered here may be synthetically accessible. Moreover, it is worth noting that recent reports indicate that Li argyrodites can be made with compositions that deviate from the traditional formula of Li_6PS_5X,[19,20,23,26] which augments the possible synthesis routes to create Na argyrodites.

Second, argyrodites in the Na−Sb−S−X systems generally have lower E_{hull} values than other systems, as clearly demonstrated by the violin plot shown in Figure 3. In the violin plot, the sodium argyrodites are divided into four groups depending on the chalcogen and pnictogen type. For each of the group, the frequency with which a certain value of E_{hull} is found is given by the width of the violin. In addition, many of the halogen-substituted compounds in Na−P−S−X systems have much higher E_{hull} values. These trends imply that the size of the pnictogen and chalcogen atoms affects the stability of these materials. More specifically, the SbS_4 polyanion seems to be easier to be formed in Na argyrodites than in the PS_4 polyanion.

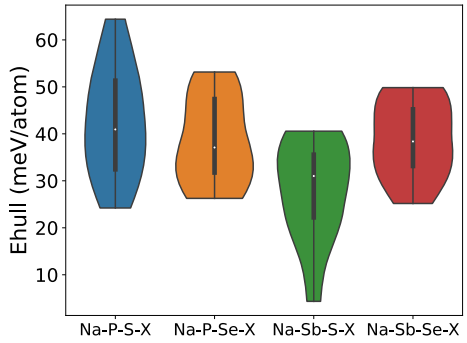

Figure 3. Distribution of E_{hull} values for different chemistries of Na argyrodites. The violin plot shows the kernel density distribution of E_{hull}, while the inner box spans the interquartile range. The violin is truncated to remain within the range of energies observed in the computations.

3.2. Electrochemical Stability. By computing the electrochemical stability window of all argyrodites, we found that the type of halogen X does not greatly affect the electrochemical stability or decomposition phases considering that the stability limits are set by the polyanion and the chalcogen. For instance, for Na_6PS_5X (X = Cl, Br, and I), the calculated stability window is (1.28, 1.59 V) for all three types of halogens. The phase equilibria at different Na chemical potentials of four compositional spaces are presented in Figure 4a−d, and the thermodynamic stability windows are shown in Figure 4e. In the stability diagrams in Figure 4a−d, the Na chemical potential (voltage) decreases (increases) from bottom to top. At each voltage, the most stable phase at the composition of the relevant argyrodite (Na_6PS_5X or $Na_5PS_4X_2$) is shown. To keep the plots readable, several compounds with similar formulas and properties were grouped, for example, sodium sulfides with sulfur at different charge states are grouped as Na_xS_y. Phases with a band gap smaller than 0.5 eV are marked in Figure 4 as potential electronic conductors which would not be passivating.[34]

It can be observed from Figure 4a−d that Na argyrodites are generally electrochemically stable within the voltage range of 1−2 V. Higher voltages are predicted to oxidize the chalcogen atom, and voltages below the stability window reduce the pnictogen atom from +5 to +3 and even to negative valence at low enough voltage. It is also worth noting that the electrochemical stability window is very narrow for Na−Sb−S(Se)−X systems. Sb-containing compounds will form metallic Sb at low voltage, making it unlikely that passivation will take

https://dx.doi.org/10.1021/acs.chemmater.9b04541
Chem. Mater. 2020, 32, 1896−1903

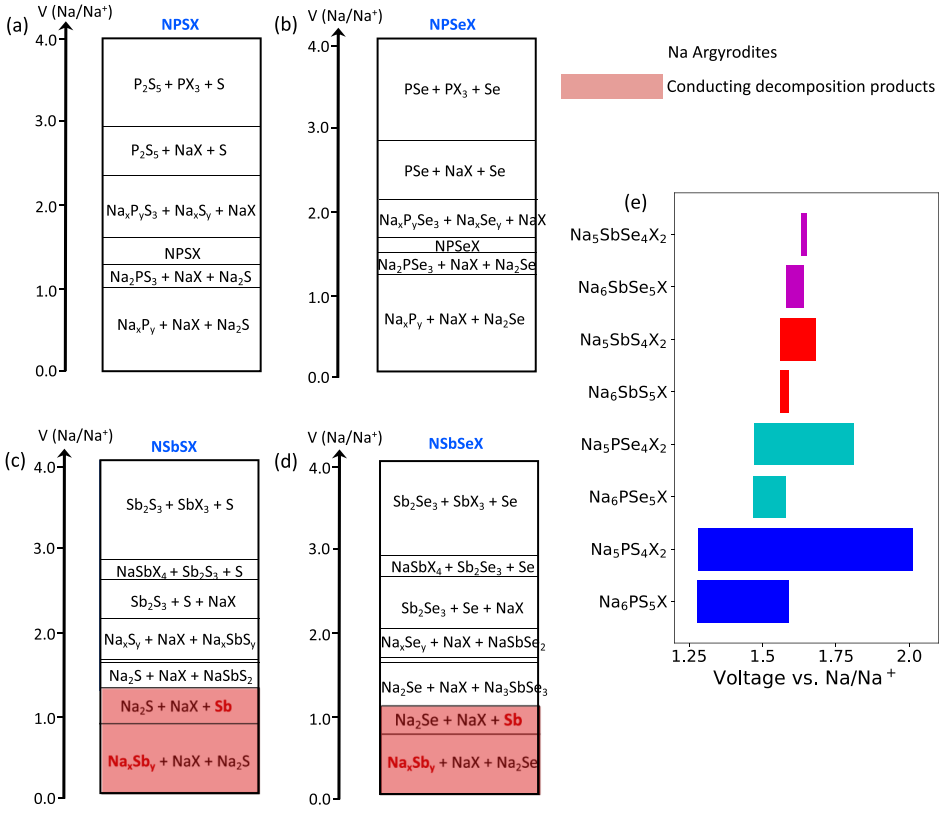

Figure 4. (a–d) Schematic demonstration of phase equilibria for sodiation and desodiation reactions for different Na argyrodites; X can be Cl, Br, or I: (a) Na–P–S–X, (b) Na–P–Se–X, (c) Na–Sb–S–X, and (d) Na–Sb–Se–X. (e) Exact voltage windows of Na argyrodites. The phases that have potentially high electronic conductivity and the voltage window in which they appear as decomposition products are colored red.

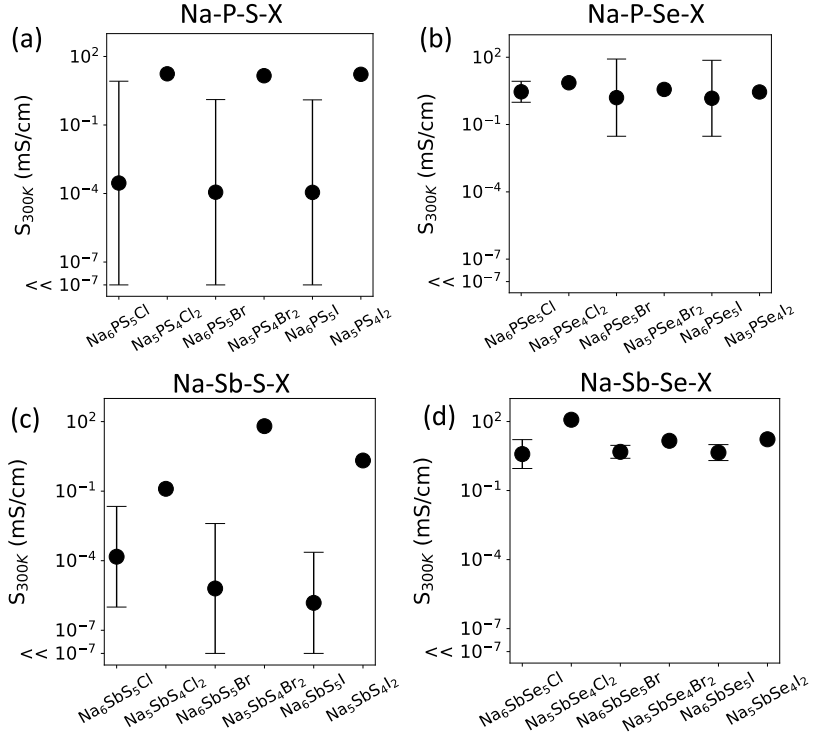

Figure 5. Distribution of room-temperature ionic conductivity for the (a) Na–P–S–X space, (b) Na–P–Se–X space, (c) Na–Sb–S–X space, and (d) Na–Sb–Se–X space. The bars indicate the range of ionic conductivities obtained with different halogen occupancies.

place. Na–P–S(Se)–X argyrodites generally have a wider electrochemical window than Sb-containing compounds. Even though they are predicted to react and decompose at both low voltage (<1 V) and high voltage (>2 V), the decomposition

https://dx.doi.org/10.1021/acs.chemmater.9b04541
Chem. Mater. 2020, 32, 1896–1903

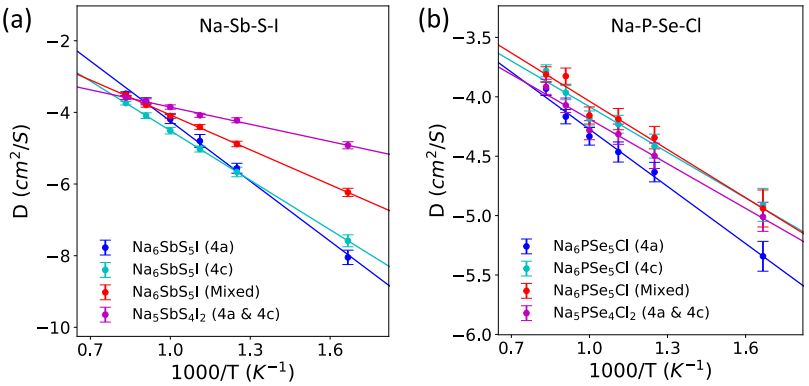

Figure 6. Arrhenius plots of two selected systems: (a) Na−Sb−S−I system with different occupancies of I and (b) Na−P−Se−Cl system with different occupancies of Cl.

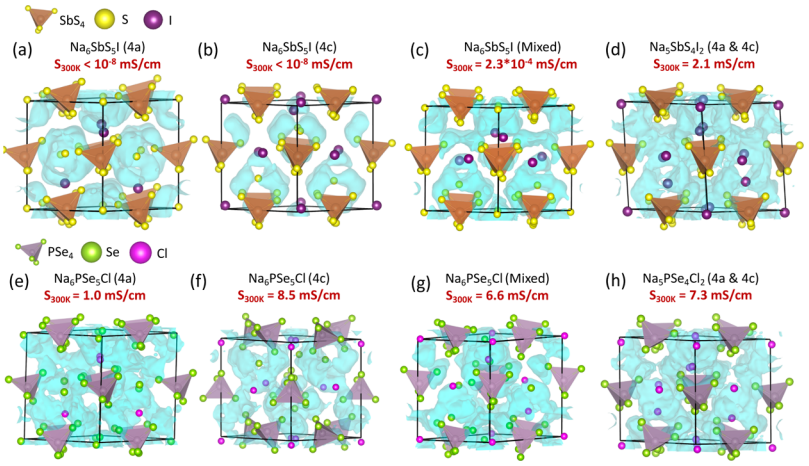

Figure 7. Isosurfaces of the Na^+ probability density distribution at 600 K with the same isosurface value of 2×10^{-4} (light blue) for (a) Na_6SbS_5I (4a), (b) Na_6SbS_5I (4c), (c) Na_6SbS_5I (mixed), (d) $Na_5SbS_4I_2$ (4a and 4c), (e) Na_6PSe_5 (4a), (f) Na_6PSe_5Cl (4c), (g) Na_6PSe_5Cl (mixed), and (h) $Na_5PSe_4Cl_2$ (4a and 4c).

products are always insulating; thus, they can potentially serve as a passivation layer that prevents further degradation.

3.3. Ionic Conductivity. The ionic conductivities of all the compounds shown in Figure 2 were calculated by performing AIMD simulations in a range of temperatures. Activation energies and estimated room-temperature conductivities are obtained from an Arrhenius fit to the *T*-dependent data. The room-temperature ionic conductivities for all compounds are shown in Figure 5. For the cases where we considered different halogen occupancies ("4a", "4c", and "mixed"), the maximum and minimum conductivity value obtained is shown by the vertical bar.

Two major trends can be extracted from the distributions of conductivity shown in Figure 5. First, for all four chemical spaces, the $Na_5AB_4X_2$-type argyrodites generally exhibit higher conductivity than all the configurations with the Na_6AB_5X composition. Second, there is a significant variation in the ionic conductivity with the site occupancy in the sulfide systems: Na−P−S−X and Na−Sb−S−X. For selenide-based systems, the conductivities do not show a strong dependence on the halogen occupancy. More specifically, in sulfide-based systems, depending on the halogen occupancy, the ionic conductivity can be very good (>10 mS/cm) or very poor ($\ll 10^{-7}$ mS/cm) for the same composition. However, for selenide-based systems, the conductivity generally remains similar regardless of the halogen occupancy. These observations suggest that the conducting mechanism in sulfide-based systems differs substantially from that in selenide systems. To further understand the origin of this difference, we selected one specific sulfide chemical space, Na−Sb−S−I, and one specific selenide chemical space, Na−P−Se−Cl, for further investigation. The Arrhenius plots for all four occupancies for both chemical spaces are presented in Figure 6 (The Arrhenius curve and conductivity for all the sodium argyrodites can be found in the Supporting Information, S3 and S4).

Figure 6a shows that in the Na−Sb−S−I system, configuration "4a" has the lowest ionic conductivity at low temperature (below 600 K), with a similar ionic conductivity for configuration "4c". However, the "mixed" configuration, with both 4a and 4c sites being half-occupied by halogens, results in much higher ionic conductivity at low temperature. Furthermore, when both 4a and 4c sites are occupied by I atoms (the "4a and 4c" case), the conductivity is the highest. It should be noted that when only the 4a and 4c sites are substituted by the halogen, the Na diffusivity is very low at low temperature. For these systems, a total simulation time of 200 ps is used to ensure proper statistics. Additionally, we evaluated the root mean deviation in the MSD fitting and the number of Na jumps to make sure that the calculations are well-converged (details in the Supporting Information, S1 and S2). As illustrated in Figure 6b, the Arrhenius plots do not differ greatly for the four configurations in the Na−P−Se−Cl

https://dx.doi.org/10.1021/acs.chemmater.9b04541
Chem. Mater. 2020, 32, 1896−1903

system. In addition, no obvious site-occupancy dependency of the conductivity is observed, as configuration "4c" results in the smallest ionic conductivity at low temperature and the "4a" and "mixed" configurations result in comparable conductivities.

4. DISCUSSION

To understand the dependence of the Na-ion conductivity on chemistry and configuration of the halogen, the Na^+ density distributions obtained from the AIMD run for Na−Sb−S−I and Na−P−Se−Cl are visualized in Figure 7. Figure 7a−d indicates that the Na mobility varies substantially with the halogen-site occupancy in Na−Sb−S−I. For both the "4a" and "4c" configurations of Na_6SbS_5I, the Na probability distribution is localized around the loosely bonded sulfur. As a result, Na moves around this S ion but does not percolate well through the structure as this requires hops between distinct Na−S clusters. In contrast, when half of the 4a and 4c sites are occupied by I atoms (Figure 7c), Na hops between clusters are easier such that Na is able to percolate more rapidly through the material. When both 4a and 4c sites are fully occupied by halogens, the Na percolation is maximized, resulting in the highest ionic conductivity. Interestingly, for the Na−P−Se−Cl system, the Na percolation is not as sensitive to the halogen-site occupancy. For all four halogen configurations in the selenide system, the Na diffusion is generally good with similar connectivity between Na clusters.

The effect of halogen-site occupancy can be understood by considering the bond length variations that halogens introduce when substituted into sulfides and selenides. In order to quantify these, we have analyzed the Na−Na distance variation in each compound and grouped the results in terms of the chalcogen type and whether only on or both 4a and 4c are substituted by a halogen. The various nearest neighbor Na−Na distances in the materials are classified as either intercluster (D_{Inter}) or intracluster (D_{Intra}), depending on whether both Na ions are part of the same Na cluster associated with a 4a or 4c anion. The range of the ratio of these two distances is plotted in Figure 8a for sulfides and selenides as a function of halogen occupancy. This descriptor helps us to quantify the difference in a local environment which Na has to experience when it changes from hopping around in the same cluster versus hopping between distinct Na clusters. In addition, we plot in Figure 8b the range of distances between the 4a and 4c sites for the various chemistries. This descriptor, which is mainly set by the anion framework, helps us to quantify the radial extent of Na clusters. As demonstrated in Figure 8a, there is a large difference between the Na−Na intracluster and intercluster distance for sulfide when only 4a or 4c is occupied by a halogen, consistent with its poorer diffusivity. This distance variation is created by the size contrast between the halogen and the sulfur. Figure 8b indicates that for the P−S compounds, the 4a−4c distance is generally the lowest among the group of chemistries we investigated. Occupying only 4a or 4c by a large lower-charged halogen in the sulfide compresses the Na cluster surrounding the other non-substituted S^{2-}. Although this compression facilitates intracluster hopping, it makes intercluster Na diffusion more difficult, as shown in Figure 7a,b, leading to a lower overall Na conductivity. Only when both 4a and 4c are fully or partially substituted by large halogens does an easy percolating pathway form. As shown by the orange bar in Figure 8a, mixed and full 4a/4c occupancy lead to a lower average ratio between inter and intra Na−Na distance, consistent with the greatly

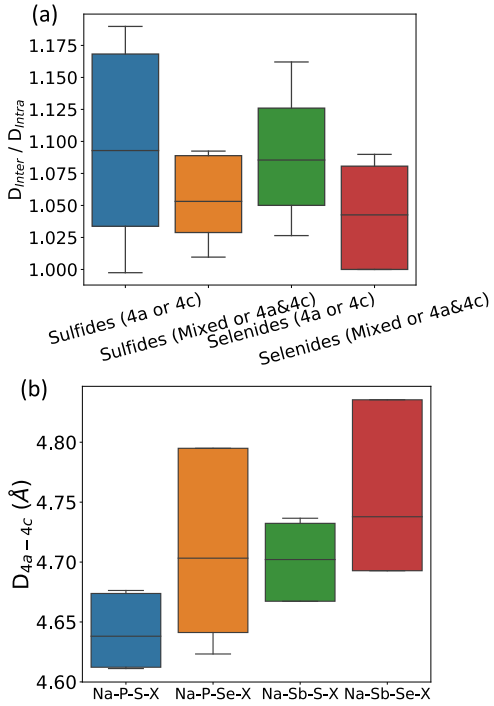

Figure 8. (a) Ratio of the intercluster Na−Na distance (D_{Inter}) and intracluster Na−Na distance (D_{Intra}) across all the evaluated Na argyrodites; (b) Distance between 4a and 4c sites across all evaluated Na argyrodites.

improved diffusion as shown in Figure 7 for Na_6SbS_5I (mixed) and $Na_5SbS_4I_2$ (4a and 4c).

The insensitivity of the selenide system to the 4a/4c halogen occupancy can also be understood in the same context. The larger ionic size of Se^{2-} ensures a larger anion framework as corroborated by the 4a−4c distance shown in Figure 8b. Consequently, the compression effect accompanied by halogen substitution is less significant in the selenides, as shown in Figure 8a, which leads to generally good ionic conductivity and less sensitivity to halogen occupancy. Stamminger et al. recently also reported on the dependence of Li conductivity in Li_6PS_5X argyrodites[25] on the site occupancy.

By comparing all four compositional spaces combining different pnictogen and chalcogen species, it can be observed that compounds in the Na−P−Se−X space generally have lower E_{hull} values than those in the Na−P−S−X space. They are also predicted to have better electrochemical stability than those in the Na−Sb−S(Se)−X family because the Na−P−Se−X compounds can be passivated by nonconducting decomposition products at both low and high voltage. In Sb-containing systems, metallic compounds are likely to be formed below the reduction limit prohibiting passivation. Additionally, in terms of experimental design, synthesizing argyrodites with precise control of the halogen site occupancy may be difficult as our calculation suggests similar energetics among different site occupancies (Figure 1), which could pose a challenge for synthesizing good sulfide argyrodites. Thus, Na−P−Se−X systems are considered more promising as they combine insensitivity of their ionic conductivity to the halogen-site occupancy with good predicted ionic conductivity.

https://dx.doi.org/10.1021/acs.chemmater.9b04541
Chem. Mater. 2020, 32, 1896−1903

5. CONCLUSIONS

Using first-principles calculations, we evaluated the phase stability, electrochemical stability, and ionic conductivity of 48 potential Na argyrodites and established an understanding of the requirements to achieve good ionic conductivity in Na argyrodites. Some of the predicted Na argyrodites exhibited both good stability and ionic conductivity, especially within the Na−P−Se−X (X = Cl, Br, or I) compositional space. We expect that this computational screening will stimulate the discovery of more Na superionic conductors for potential application as electrolytes in solid-state batteries.

■ ASSOCIATED CONTENT

Supporting Information

The Supporting Information is available free of charge at https://pubs.acs.org/doi/10.1021/acs.chemmater.9b04541.

R^2 fitting errors of MSD for the Na−Sb−S−I system and Na−P−Se−Cl system; number of intercluster jumps for the Na−Sb−S−I system and Na−P−Se−Cl system; Arrhenius plot for all sodium argyrodites considered; and room-temperature Na^+ conductivity for all sodium argyrodites considered (PDF)

■ AUTHOR INFORMATION

Corresponding Author

Gerbrand Ceder − *Department of Materials Science and Engineering, University of California, Berkeley, Berkeley, California 94720, United States; Materials Science Division, Lawrence Berkeley National Laboratory, Berkeley, California 94720, United States;* orcid.org/0000-0001-9275-3605; Email: gceder@berkeley.edu

Authors

Bin Ouyang − *Department of Materials Science and Engineering, University of California, Berkeley, Berkeley, California 94720, United States; Materials Science Division, Lawrence Berkeley National Laboratory, Berkeley, California 94720, United States;* orcid.org/0000-0002-8181-6815

Yan Wang − *Advanced Materials Lab, Samsung Research America, Burlington, Massachusetts 01803, United States;* orcid.org/0000-0002-8648-2172

Yingzhi Sun − *Department of Materials Science and Engineering, University of California, Berkeley, Berkeley, California 94720, United States; Materials Science Division, Lawrence Berkeley National Laboratory, Berkeley, California 94720, United States*

Complete contact information is available at: https://pubs.acs.org/10.1021/acs.chemmater.9b04541

Notes

The authors declare no competing financial interest.

■ ACKNOWLEDGMENTS

This work was funded by the Samsung Advanced Institute of Technology. The computational analysis was performed using computational resources sponsored by the Department of Energy's Office of Energy Efficiency and Renewable Energy at the National Renewable Energy Laboratory. Computational resources were also provided by the Extreme Science and Engineering Discovery Environment (XSEDE), which is supported by the National Science Foundation grant number ACI1053575 and the National Energy Research Scientific Computing Center (NERSC), a DOE Office of Science User Facility supported by the Office of Science and the U.S. Department of Energy under contract no. DE-AC02-05CH11231.

■ REFERENCES

(1) Bron, P.; Johansson, S.; Zick, K.; Schmedt auf der Günne, J.; Dehnen, S.; Roling, B. Li10SnP2S12: An Affordable Lithium Superionic Conductor. *J. Am. Chem. Soc.* **2013**, *135*, 15694−15697.

(2) Ceder, G.; Ong, S. P.; Wang, Y. Predictive modeling and design rules for solid electrolytes. *MRS Bull.* **2018**, *43*, 746−751.

(3) Kamaya, N.; Homma, K.; Yamakawa, Y.; Hirayama, M.; Kanno, R.; Yonemura, M.; Kamiyama, T.; Kato, Y.; Hama, S.; Kawamoto, K.; Mitsui, A. A lithium superionic conductor. *Nat. Mater.* **2011**, *10*, 682.

(4) Miara, L. J.; Suzuki, N.; Richards, W. D.; Wang, Y.; Kim, J. C.; Ceder, G. Li-ion conductivity in Li9S3N. *J. Mater. Chem. A* **2015**, *3*, 20338−20344.

(5) Murugan, R.; Thangadurai, V.; Weppner, W. Fast Lithium Ion Conduction in Garnet-Type Li7La3Zr2O12. *Angew. Chem., Int. Ed.* **2007**, *46*, 7778−7781.

(6) Ohta, S.; Kobayashi, T.; Asaoka, T. High lithium ionic conductivity in the garnet-type oxide Li7−X La3(Zr2−X, NbX)O12 (X=0−2). *J. Power Sources* **2011**, *196*, 3342−3345.

(7) Ong, S. P.; Mo, Y.; Richards, W. D.; Miara, L.; Lee, H. S.; Ceder, G. Phase stability, electrochemical stability and ionic conductivity of the Li10±1MP2X12 (M = Ge, Si, Sn, Al or P, and X = O, S or Se) family of superionic conductors. *Energy Environ. Sci.* **2013**, *6*, 148−156.

(8) Richards, W. D.; Tsujimura, T.; Miara, L. J.; Wang, Y.; Kim, J. C.; Ong, S. P.; Uechi, I.; Suzuki, N.; Ceder, G. Design and synthesis of the superionic conductor Na10SnP2S12. *Nat. Commun.* **2016**, *7*, 11009.

(9) Richards, W. D.; Wang, Y.; Miara, L. J.; Kim, J. C.; Ceder, G. Design of Li1+2xZn1−xPS4, a new lithium ion conductor. *Energy Environ. Sci.* **2016**, *9*, 3272−3278.

(10) Seino, Y.; Ota, T.; Takada, K.; Hayashi, A.; Tatsumisago, M. A sulphide lithium super ion conductor is superior to liquid ion conductors for use in rechargeable batteries. *Energy Environ. Sci.* **2014**, *7*, 627−631.

(11) Suzuki, N.; Richards, W. D.; Wang, Y.; Miara, L. J.; Kim, J. C.; Jung, I.-S.; Tsujimura, T.; Ceder, G. Synthesis and Electrochemical Properties of $I\bar{4}$-Type Li1+2xZn1−xPS4 Solid Electrolyte. *Chem. Mater.* **2018**, *30*, 2236−2244.

(12) Wang, Y.; Richards, W. D.; Bo, S.-H.; Miara, L. J.; Ceder, G. Computational Prediction and Evaluation of Solid-State Sodium Superionic Conductors Na7P3X11 (X = O, S, Se). *Chem. Mater.* **2017**, *29*, 7475−7482.

(13) Wang, Y.; Richards, W. D.; Ong, S. P.; Miara, L. J.; Kim, J. C.; Mo, Y.; Ceder, G. Design principles for solid-state lithium superionic conductors. *Nat. Mater.* **2015**, *14*, 1026.

(14) Lü, X.; Howard, J. W.; Chen, A.; Zhu, J.; Li, S.; Wu, G.; Dowden, P.; Xu, H.; Zhao, Y.; Jia, Q. Antiperovskite Li3OCl Superionic Conductor Films for Solid-State Li-Ion Batteries. *Adv. Sci.* **2016**, *3*, 1500359.

(15) Sun, Y.; Wang, Y.; Liang, X.; Xia, Y.; Peng, L.; Jia, H.; Li, H.; Bai, L.; Feng, J.; Jiang, H.; Xie, J. Rotational Cluster Anion Enabling Superionic Conductivity in Sodium-Rich Antiperovskite Na3OBH4. *J. Am. Chem. Soc.* **2019**, *141*, 5640−5644.

(16) Fang, H.; Jena, P. Li-rich antiperovskite superionic conductors based on cluster ions. *Proc. Natl. Acad. Sci.* **2017**, *114*, 11046−11051.

(17) Allen, J. L.; Wolfenstine, J.; Rangasamy, E.; Sakamoto, J. Effect of substitution (Ta, Al, Ga) on the conductivity of Li7La3Zr2O12. *J. Power Sources* **2012**, *206*, 315−319.

(18) Yamauchi, A.; Sakuda, A.; Hayashi, A.; Tatsumisago, M. Preparation and ionic conductivities of (100 − x)(0.75Li2S·0.25P2S5)·xLiBH4 glass electrolytes. *J. Power Sources* **2013**, *244*, 707−710.

(19) Kraft, M. A.; Ohno, S.; Zinkevich, T.; Koerver, R.; Culver, S. P.; Fuchs, T.; Senyshyn, A.; Indris, S.; Morgan, B. J.; Zeier, W. G.

Inducing High Ionic Conductivity in the Lithium Superionic Argyrodites Li6+xP1−xGexS5I for All-Solid-State Batteries. *J. Am. Chem. Soc.* **2018**, *140*, 16330−16339.
(20) Zhou, L.; Park, K.-H.; Sun, X.; Lalère, F.; Adermann, T.; Hartmann, P.; Nazar, L. F. Solvent-Engineered Design of Argyrodite Li6PS5X (X = Cl, Br, I) Solid Electrolytes with High Ionic Conductivity. *ACS Energy Lett.* **2019**, *4*, 265−270.
(21) de Klerk, N. J. J.; Rosłoń, I.; Wagemaker, M. Diffusion Mechanism of Li Argyrodite Solid Electrolytes for Li-Ion Batteries and Prediction of Optimized Halogen Doping: The Effect of Li Vacancies, Halogens, and Halogen Disorder. *Chem. Mater.* **2016**, *28*, 7955−7963.
(22) Deiseroth, H.-J.; Kong, S.-T.; Eckert, H.; Vannahme, J.; Reiner, C.; Zaiß, T.; Schlosser, M. Li6PS5X: A Class of Crystalline Li-Rich Solids With an Unusually High Li+ Mobility. *Angew. Chem., Int. Ed.* **2008**, *47*, 755−758.
(23) Adeli, P.; Bazak, J. D.; Park, K. H.; Kochetkov, I.; Huq, A.; Goward, G. R.; Nazar, L. F. Boosting Solid-State Diffusivity and Conductivity in Lithium Superionic Argyrodites by Halide Substitution. *Angew. Chem., Int. Ed.* **2019**, *58*, 8681−8686.
(24) Chen, H. M.; Maohua, C.; Adams, S. Stability and ionic mobility in argyrodite-related lithium-ion solid electrolytes. *Phys. Chem. Chem. Phys.* **2015**, *17*, 16494−16506.
(25) Stamminger, A. R.; Ziebarth, B.; Mrovec, M.; Hammerschmidt, T.; Drautz, R. Ionic Conductivity and Its Dependence on Structural Disorder in Halogenated Argyrodites Li6PS5X (X = Br, Cl, I). *Chem. Mater.* **2019**, *31*, 8673−8678.
(26) Zhou, L.; Assoud, A.; Zhang, Q.; Wu, X.; Nazar, L. F. New Family of Argyrodite Thioantimonate Lithium Superionic Conductors. *J. Am. Chem. Soc.* **2019**, *141*, 19002−19013.
(27) Kong, S. T.; Gün, Ö.; Koch, B.; Deiseroth, H. J.; Eckert, H.; Reiner, C. Structural Characterisation of the Li Argyrodites Li7PS6 and Li7PSe6 and their Solid Solutions: Quantification of Site Preferences by MAS-NMR Spectroscopy. *Chem.—Eur. J.* **2010**, *16*, 5138−5147.
(28) Kresse, G.; Furthmüller, J. Efficient iterative schemes for ab initio total-energy calculations using a plane-wave basis set. *Phys. Rev. B: Condens. Matter Mater. Phys.* **1996**, *54*, 11169−11186.
(29) Perdew, J. P.; Burke, K.; Ernzerhof, M. Generalized Gradient Approximation Made Simple. *Phys. Rev. Lett.* **1996**, *77*, 3865−3868.
(30) Hautier, G.; Fischer, C.; Ehrlacher, V.; Jain, A.; Ceder, G. Data Mined Ionic Substitutions for the Discovery of New Compounds. *Inorg. Chem.* **2011**, *50*, 656−663.
(31) Sun, W.; Dacek, S. T.; Ong, S. P.; Hautier, G.; Jain, A.; Richards, W. D.; Gamst, A. C.; Persson, K. A.; Ceder, G. The thermodynamic scale of inorganic crystalline metastability. *Sci. Adv.* **2016**, *2*, No. e1600225.
(32) Miara, L. J.; Richards, W. D.; Wang, Y. E.; Ceder, G. First-Principles Studies on Cation Dopants and Electrolyte|Cathode Interphases for Lithium Garnets. *Chem. Mater.* **2015**, *27*, 4040−4047.
(33) Richards, W. D.; Miara, L. J.; Wang, Y.; Kim, J. C.; Ceder, G. Interface Stability in Solid-State Batteries. *Chem. Mater.* **2016**, *28*, 266−273.
(34) Xiao, Y.; Miara, L. J.; Wang, Y.; Ceder, G. Computational Screening of Cathode Coatings for Solid-State Batteries. *Joule* **2019**, *3*, 1252−1275.
(35) Lacivita, V.; Wang, Y.; Bo, S.-H.; Ceder, G. Ab initio investigation of the stability of electrolyte/electrode interfaces in all-solid-state Na batteries. *J. Mater. Chem. A* **2019**, *7*, 8144−8155.
(36) Aydinol, M. K.; Kohan, A. F.; Ceder, G. Ab initio calculation of the intercalation voltage of lithium-transition-metal oxide electrodes for rechargeable batteries. *J. Power Sources* **1997**, *68*, 664−668.
(37) Aydinol, M. K.; Ceder, G. First-Principles Prediction of Insertion Potentials in Li-Mn Oxides for Secondary Li Batteries. *J. Electrochem. Soc.* **1997**, *144*, 3832−3835.
(38) Aydinol, M. K.; Kohan, A. F.; Ceder, G.; Cho, K.; Joannopoulos, J. Ab initio study of lithium intercalation in metal oxides and metal dichalcogenides. *Phys. Rev. B: Condens. Matter Mater. Phys.* **1997**, *56*, 1354−1365.
(39) Nosé, S. A unified formulation of the constant temperature molecular dynamics methods. *J. Chem. Phys.* **1984**, *81*, 511−519.
(40) Deng, Z.; Zhu, Z.; Chu, I.-H.; Ong, S. P. Data-Driven First-Principles Methods for the Study and Design of Alkali Superionic Conductors. *Chem. Mater.* **2017**, *29*, 281−288.

https://dx.doi.org/10.1021/acs.chemmater.9b04541
Chem. Mater. 2020, 32, 1896−1903